Arch. Mech., 38, 4, pp. 439–462, Warszawa 1986

Properties of pure hysteresis behaviour of solids Case of stainless steel and superalloy

S. HAN (BEIJING) and B. WACK (GRENOBLE)

PURE HYSTERESIS behaviour is recognized as the leading phenomenon in solid behaviour. Its properties are made conspicuous by an analysis of cyclic test results in traction and torsion, with a stainless steel ICL 167 SPH and a superalloy Inco 718, and concern: the notion of discrete memory, the irreversibility of the deformation from the beginning; no boundary between an elastic and a plastic domain can be determined; elastic behaviour is tangential behaviour at the origin of each loading branch. The shape of the loading surface is axisymmetrical for the stainless steel, but not for the superalloy; a nonsymmetrical rheological model is analysed. Some explanations at the microstructural scale confirm the properties at the macroscopical scale.

Czystą histerezę uważa się za podstawowe zjawisko w zachowaniu się ciał stałych. Cechy tego zjawiska można uwidocznić, analizując cykliczne próby rozciągania i skręcania próbek ze stali nierdzewnej ICL 167 SPH i nadstopu Inco 718; dotyczą one pojęcia pamięci dyskretnej i nieodwracalności odkształcenia; nie można ustalić granicy między obszarami plastycznymi i sprężystymi; zachowanie sprężyste ma charakter styczny na początku każdej gałęzi obciążania. Kształt powierzchni obciążania jest osiowo-symetryczny dla stali nierdzewnej, inaczej niż w przypadku nadstopu; przeanalizowano niesymetryczny model reologiczny. Pewne wyjaśnienia dotyczące skali mikrostrukturalnej potwierdzają te własności dla przypadku skali makroskopowej.

Чистый гистерезис считается основным явлением в поведении твердых тел. Свойства этого явления можно представить, анализируя циклические испытания растяжения и скручивания образцов из нержавеющей стали ICL 167 SPH и сверхсплава Inco 718; касаются они понятия дискретной памяти и необратимости деформации; нельзя определить границы между пластическими и упругими областями; упругое поведение имеет касательный характер вначале каждой ветви нагружения. Форма поверхности нагружения является осесимметричной для нержавеющей стали, иначе чем в случае сверхсплава; проанализирована несимметричная реологическая модель. Некоторые выяснения, касающиеся микроструктурного масштаба, подтверждают эти свойства для случая макроскопического масштаба.

1. Introduction

IN MOST OF THE ADVANCED technological applications, material solicitations are often of the cyclic type and reach a stress level where the nonlinearity of the material behaviour is important. Thus the force-displacement or the stress-strain diagram describes a quite wide hysteresis loop; this loop can be closed or opened depending on the test conditions.

A closed hysteresis loop characterizes the phenomenon of mechanical pure hysteresis related to the microstructural phenomenon of solid friction. During the material solicitation other phenomena can also take place, like the strain hardening phenomenon which is importat for stainless steel, or the viscosity phenomenon which is responsible for the creep or relaxation aspects of the macroscopical behaviour.

When the scientist or the engineer wants to modelize such a complicated behaviour it is important to know if all these phenomena are of equal importance, or if one is a leading phenomenon, the other one being considered as perturbating the leading phenomenon. In trying to give an answer to this question, consider the evolution of the hysteresis loop in a classical push-pull test. At the beginning the cycle increases until a stable level is reached; this happens after about twenty to forty cycles. Then the stable cycle is repeated during a long time before the damage phenomenon takes place, preceding the rupture of the sample. Thus we verify that during about 95% of the sample life its behaviour shows a stable and closed hysteresis loop.

Consequently, we have to consider the fact that the phenomenon of mechanical hysteresis represents the main aspect of material behaviour. And we also have to take into account the other phenomena like strain hardening or viscosity, play the role of phenomena perturbing the leading phenomenon of mechanical hysteresis.

A model which gives a response of pure hysteresis like mechanical hysteresis is represented by rheological models with springs and sliders. Since the first study done by MASING [1], these models are well known by mechanical people who try to modelize macroscopic material behaviour. Presently metallurgists also utilize these models to explain material behaviour from the dislocation scale [2, 3]. Only recently has a complete interpretation of these rheological models been made from the classical, mechanical point of view as well as from the thermodynamical point of view [4] (see also [5, 6]).

This interpretation of pure hysteresis behaviour introduces the important notion of discrete memory of the past inversion states. It follows that the stress appears with the argument $\Delta\sigma = \sigma - {}_R\sigma$ where the reference stress ${}_R\sigma$ is a functional of the solicitation, the value of which is chosen among all the inversion states of the past; the value of ${}_R\sigma$ is piece-wise constant. Finally, the behaviour is described by a scheme constituted of three essential parts:

a) a constitutive equation with solicitation functionals as argument;

b) an inversion criterion which is able to define the inversion states in three-dimensional stress states; this criterion is the expression of the second law of thermodynamics;

c) an algorithm which defines at any time the functional values of the constitutive equation.

The main feature of this pure hysteresis behaviour consists of the notion of discrete memory, the property restoration after an inversion state, and the possibility of not using the notion of boundary between an elastic and plastic domain.

If this rheological model really represents the behaviour foundation for the real material, we have to recognize the pure hysteresis properties in the real material. Due to the presence of the other phenomena, some particular precautions have to be taken. Thus for stainless steel the viscosity influence is almost always present, even for our test conditions at room temperature and at a low strain rate of the order of $3 \cdot 10^{-5}$ s^{-1} [7, 8]. But by doing all the tests at the same low strain rate it is possible to consider the fact that the experimental results represent a valuable data body to study nonviscous behaviour.

In the following section the details of the experimental conditions and the description of the material used are given. The properties of the loading branches are analysed in

the third section and details about the curve fitting are given. Section 4 deals with the question of a small cycle described within a stable large cycle. And in the last section the shape of the asymptotic loading surface is studied.

2. Experimental conditions

Experimental data were obtained with a tube sample loaded in two directions by a servo-controlled hydraulic machine. Two materials were tested. The AISI 316L type stainless steel, the exact denomination of which is ICL 167 SPH, is used in the nuclear reactors industry, due to its good resistance to corrosion and creep at the utilization temperature of about 550°C. The second metal is a superalloy of nickel base Inco 718; this alloy presents a high strength at the elevated temperature of utilization in the turbines of the aeronautical industry. Details on the experimental conditions are given in [11]. We recall here only some particular points necessary for our explanations.

All the tests are run at room temperature; they are strain-controlled, the strain rate being of the order of 3.10^{-5} s^{-1}. The deformation of the cylindrical part of the sample is measured with a set of three strain gages at an orientation of 45°.

The strain measurements given by the strain gauges are not strictly equal to the strain tensor components. The difference is important for the axial strain in the case of a torsion test [8, 9]. To remain homogeneous with previous and forthcoming papers, we will use here the notation λ_{ij} to represent the measurements of the strain gauges. By using a cylindrical coordinate system (radius ϱ, angle θ and axial position z), the strain gauge set is able to measure the three components: λ_{zz}, $\lambda_{\theta\theta}$ and $\lambda_{\theta z}$.

During a torsion test, the shear stress distribution evolves theoretically from a linear variation with the radius to a constant value [10]. For simplicity we consider here a tube thin enough to neglect these variations. The axial stress is corrected from the cross-section variation. Thus we have

$$\sigma_{zz} = \frac{F_z}{S_0(1+\lambda_{\theta\theta})^2} \quad \text{and} \quad \sigma_{\theta z} = <\sigma_{\theta z}> \equiv \frac{3}{2\pi}\frac{C}{R_e^3 - R_i^3},$$

where F_z is the axial force, C the torque, S_0 the initial cross section, R_e and R_i the outside and inside radius, respectively.

3. Loading branches properties

Since the data are registered by a microprocessor, it is possible to determine the properties of the loading branches using of a curve fitting technique; this enables us to determine essentially the value of the derivative and its evolution along the loading branch.

3.1. The method of analysis

The data are separated by branches, each corresponding to a segment of loading path comprised between two inversion states. Each branch is analysed in the space $\Delta\sigma$, $\Delta\lambda$ with

$$\Delta\sigma = \sigma - {}_R\sigma \quad \text{and} \quad \Delta\lambda = \lambda - {}_R\lambda,$$

where ${}_R\sigma$, ${}_R\lambda$ are the coordinates of the reference state.

With the simple solicitations used here, (see for example Fig. 1) the reference state ${}_R\sigma$, ${}_R\lambda$ is in most cases the inversion state of the beginning of each branch. Since the inversion point does not correspond exactly to a data point, ${}_R\sigma$ and ${}_R\lambda$ are the coordinates of the first data point after an inversion; due to the high frequency of the data pick up

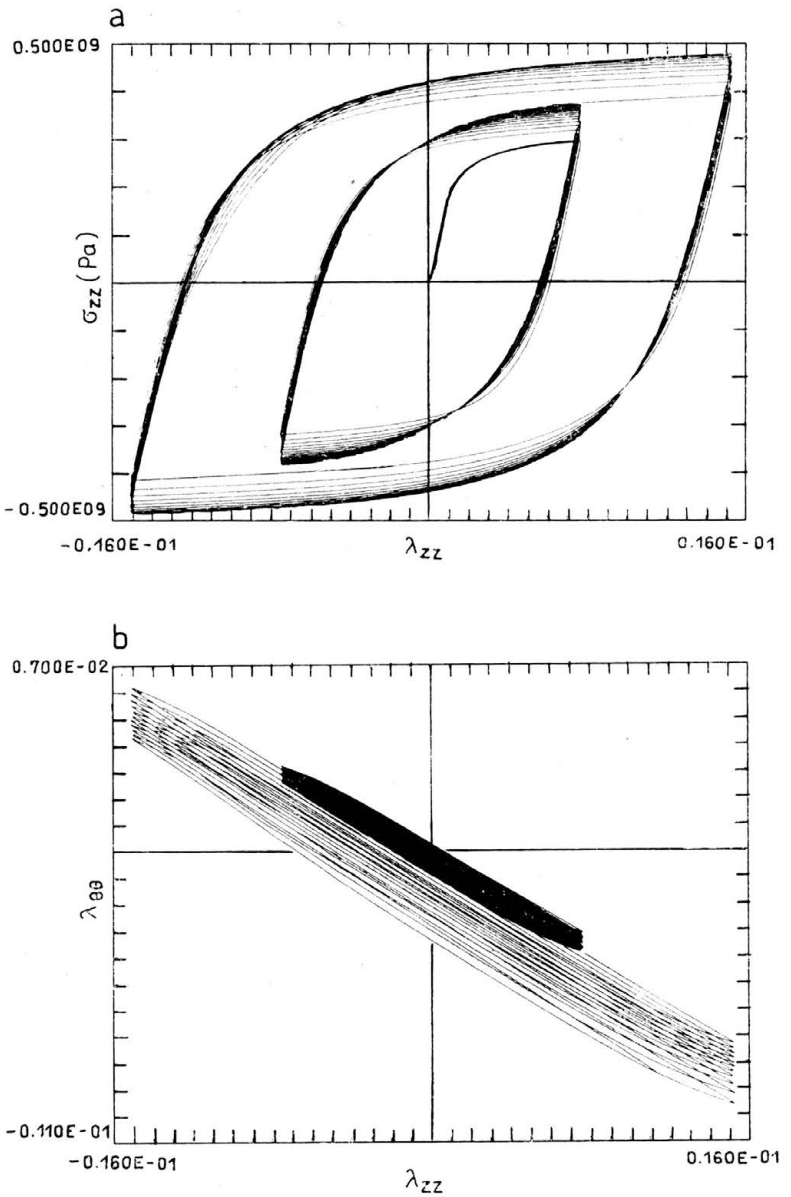

FIG. 1. Push-pull test. Axial stress (a) and circumferential strain (b) versus axial strain. Stainless steel.

this assumption will have a negligible effect: each loading branch is defined by a set of 50 to 100 data points and the strain interval between two data points is less than 10^{-4}.

The curve fitting technique used is a spline with tension allowing to modelize the experimental points by a smooth curve. The spline tension is adjusted by a coefficient whose value is chosen so as to just make the experimental scattering disappear, the field of adjustment being comprised between the two extreme cases of interpolation and of the mean square straight line. Thus the adjusted curve is always inside the band of experimental scattering whose width is ± 0.2 MPa. It is then possible to determine the tangent of the following curves and the values of the modulus M_E and M_μ and of the coefficient C_ν:

for the push-pull test:

$$M_E = \frac{d\Delta\sigma_{zz}}{d\Delta\lambda_{zz}}, \qquad C_\nu = -\frac{d\Delta\lambda_{\theta\theta}}{d\Delta\lambda_{zz}};$$

for the torsion test:

$$M_\mu = \frac{1}{2}\frac{d\Delta\sigma_{\theta z}}{d\Delta\lambda_{\theta z}}.$$

The accuracy of the slopes value can be characterized by the influence of the adjustment coefficient around the retained value: thus the relative error on the determination of the modulus M_E and M_μ is less than $\pm 0.7\%$ and the relative error on the coefficient C_ν is less than $\pm 0.5\%$.

3.2. Stainless steel results

A typical push-pull test result with stainless steel is given in Fig. 1, with symmetric cycles of small amplitude $\pm 0.75\%$, followed by cycles of large amplitude $\pm 1.5\%$. The evolution of the stress $\Delta\sigma_{zz}$ and of modulus M_E for the small cycles is given in Fig. 2.

The beginning of all the loading branches is identical; this is made conspicuous by the constant M_E value at the origin; the scattering in the quasi-plastic region, for $\Delta\lambda_{zz}$ greater than 1%, is due essentially to the hardening phenomenon. The evolution of the tangential modulus M_E shows no discontinuity, and the value at the beginning is the same for all branches (Fig. 2b). At a strain difference of 0.2% the tangential modulus represents only 10% of the initial value for the first loading branch and 60% for the other branches. The initial part of the M_E curve is parabolic with a slope at the origin parallel to the strain axis; thus the loading branch is well represented in that region by a polynom of degree three:

$$\Delta\sigma_{zz} = E \cdot \Delta\lambda_{zz} - k \cdot \Delta\lambda_{zz}^3, \tag{3.1}$$

where the constant E is the limit value of M_E for $\Delta\lambda_{zz} \to 0$ and k is a positive constant. As we will see later the constant E has the meaning of a Young modulus of an elastic behaviour.

Despite the presence of strain hardening, we can see that the Masing rule roughly applies; indeed if we transform the $\Delta\sigma(\Delta\lambda)$ curve of the first loading branch by a similarity coefficient of two, the curve will join the group of the other branches and take the first

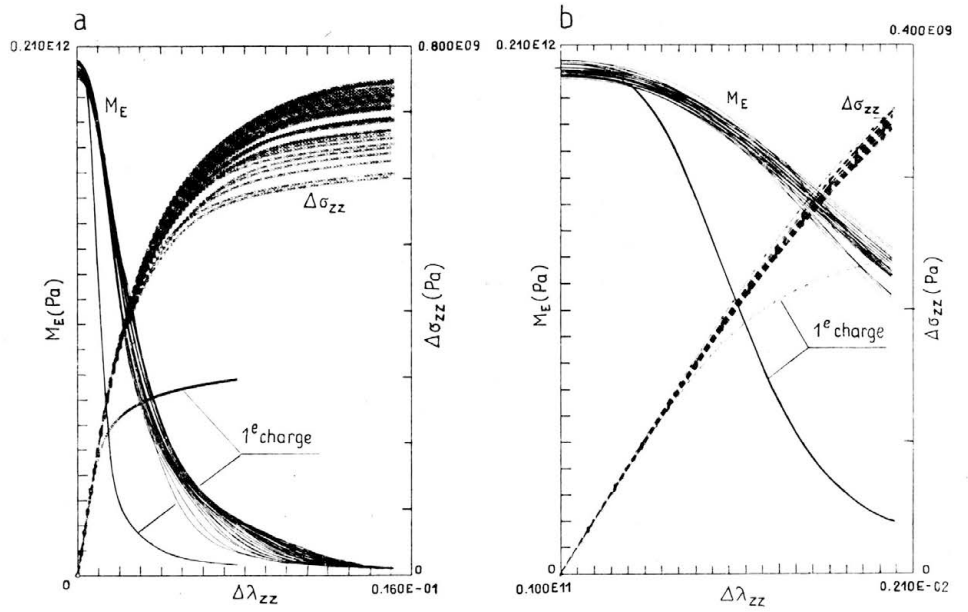

FIG. 2. Push-pull test. Variation of stress difference $\Delta\sigma_{zz}$ and modulus M_E for the small cycles, a) whole interval 0–1.6%; b) enlargement of interval 0–0.2%. Stainless steel.

place in that group (Fig. 2a). Likewise, an affine transformation pushes the $M_E(\Delta\lambda_{zz})$ first loading branch into the pile of other branches.

Strain hardening has almost no influence on the evolution of the circumferential strain (Fig. 3). The coefficient C_ν evolves continuously between a value of about 0.28 just after an inversion point to a value comprised between 0.44 and 0.48 in the quasi-plastic region. The beginning of the C_ν $(\Delta\lambda_{zz})$ curves is also parabolic with a tangent at the origin parallel to the axial strain axis.

We have to notice that the $\lambda_{\theta\theta}$ strain evolution shows a ratchet effect in the negative direction (Fig. 1); this is always confirmed by all our push-pull tests (Fig. 6) and seems to be independent of the sample cylindrical part height [8]. Unfortunately no satisfactory explanation can be done for the moment; more systematic tests have to be run to clear that point.

The analysis of a symmetric cyclic torsion test shows the same type of results (Fig. 4) as the one obtained with a push-pull test: the loading branches are continuous at least of the third order, the slope after inversion is the same for all branches and the Masing similarity rule applies. So the initial part of the loading branches can be represented by an equation like (3.1). For this test we see that the loading branches for the large cycles ($\Delta\lambda_{\theta z} = \pm 0.9\%$) have the same properties as the one for the small cycles ($\Delta\lambda_{\theta z} = \pm 0.45\%$), except that they are longer. Similar results with push-pull tests were also obtained [8].

The results of Figs. 2b and 4b show evidently that the elastic behaviour of such a stainless steel is a behaviour tangent to the origin of each branch. The initial values of the slopes define the coefficient of the tangent elasticity:

$$\lim_{\Delta\lambda_{zz}\to 0} M_E = E \quad \text{and} \quad \lim_{\Delta\lambda_{zz}\to 0} C_\nu = \nu,$$

$$\lim_{\Delta\lambda_{\theta z}\to 0} M_\mu = \mu,$$

where E is the Young's modulus, ν the Poisson's ratio and μ one of the Lamé's coefficients.

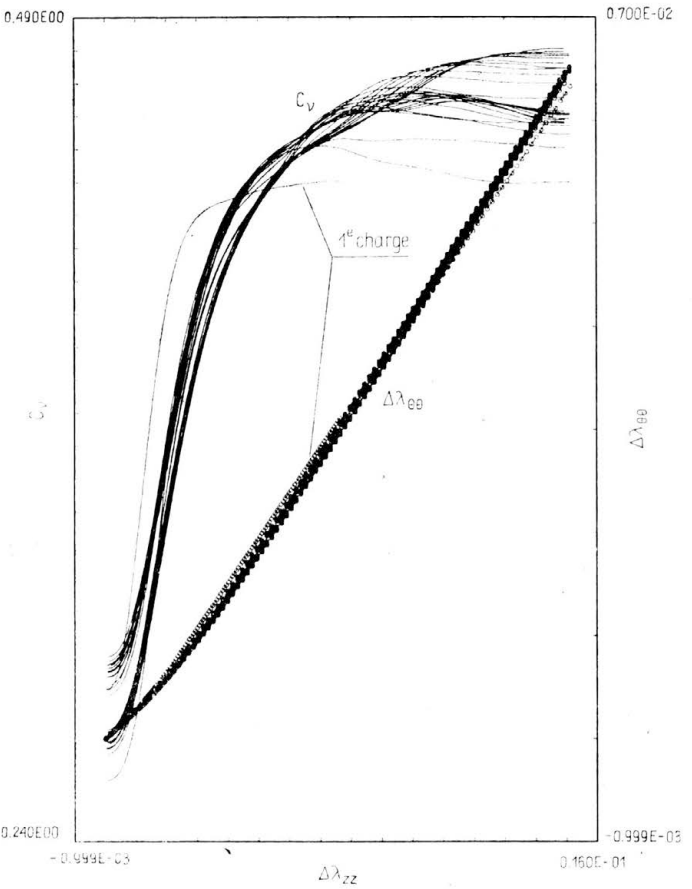

FIG. 3. Push-pull test. Variation of circumferential strain difference $\Delta\lambda_{\theta\theta}$ and coefficient C_ν versus axial strain difference $\Delta\lambda_{zz}$. Stainless steel.

Using the preceding results and complementary results with the same material [8], we obtain for the stainless steel

$$E = 199 \pm 2 \text{ GPa}, \quad \nu = 0.280 \pm 0.015, \quad \mu = 77.6 \pm 1.1 \text{ GPa}$$

the error interval being the scattering of the mean value per test. These three values are determined independently of each other and we check to see if they are consistent; for example we have

$$\mu^* = \frac{E}{2(1+\nu)} = 77.7 \text{ GPa} \tag{3.2}$$

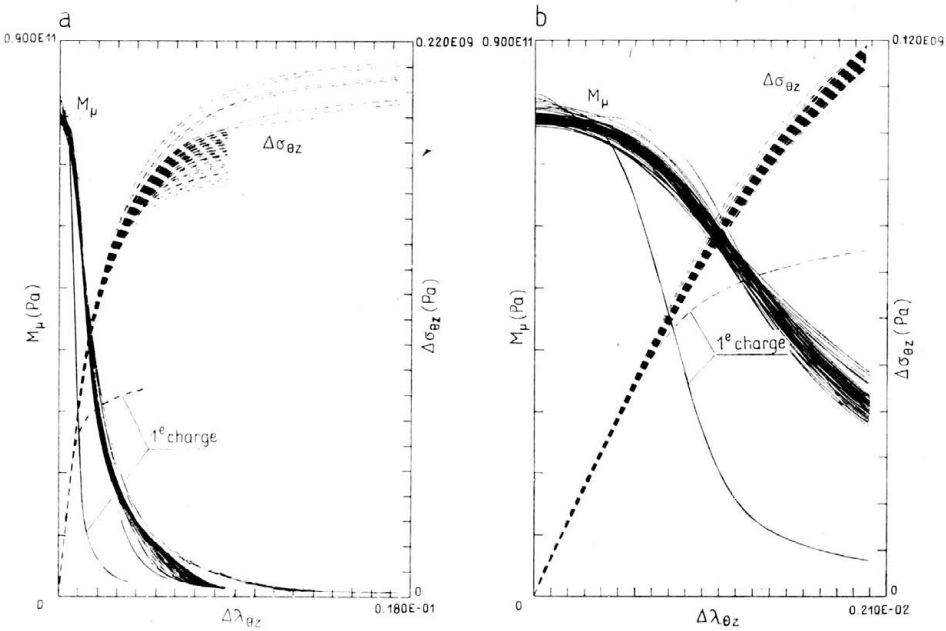

FIG. 4. Cyclic torsion test. Variation of stress difference $\Delta\sigma_{\theta z}$ and modulus M_μ versus shear strain difference, a) whole interval 0–1.8%; b) enlargement of interval 0–0.2%. Stainless steel.

and we see that this calculated value is within the error interval of the experimentally determined Lamé's coefficient.

To confirm the results obtained with the two preceding simple type tests, a combined proportional traction torsion test was run with the following values of the small cycle amplitude [8]:

$$\lambda_{zz} = \pm 0.4\% \quad \text{and} \quad \lambda_{\theta z} = \pm 0.3\%.$$

The variation of the modulus M_E and M_μ in the strain interval 0–0.2% and of the coefficient C_ν in the whole interval 0–0.8% are given in Fig. 5; these results show essentially the same properties as for the simple tests and we verify that the initial values correspond to the preceding ones. We notice, however, that the C_ν coefficient reaches a value greater than 0.5 in the quasi-plastic state; as for the simple push-pull test this coefficient always stays under this value (Figs. 3 and 8).

Indeed for a simple push-pull test we may assume the homogeneity of the stress and strain state in the annular tube cross-section and the equality of the radial and circumferential strain. With the hypothesis of small strain, the rate of the relative volume variation per branch is then given by

$$\frac{d\dfrac{\Delta V}{V}}{dt} = (1-2C_\nu)\frac{d\Delta\lambda_{zz}}{dt}. \tag{3.3}$$

Thus for the analysis of volume variation, the coefficient C_ν can be interpreted in simple push-pull tests like the Poissons's ratio ν in elasticity. Consequently, we see that the rate

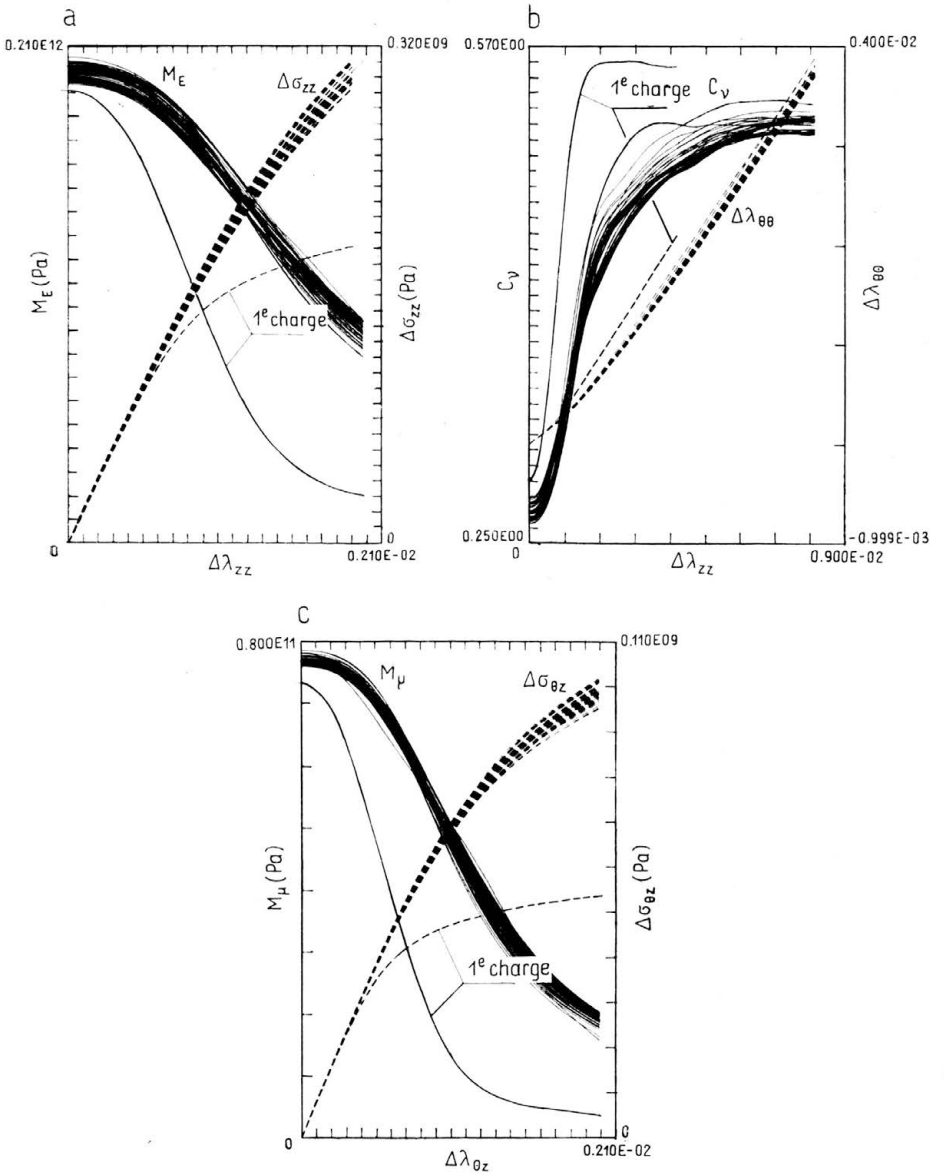

FIG. 5. Combined traction torsion test. Variation of modulus M_E a), coefficient C_ν b) and modulus M_μ c) versus strain difference. Stainless steel.

of the volume variation along any loading branch is maximum in the quasi-elastic state just after an inversion point and tends to be null in the quasi-plastic state. On the opposite, for the combined traction-torsion state the radial strain is not equal to the circumferential strain; thus Eq. (3.3) applies no more and a value C_ν slightly greater than 0.5 may theoretically be admissible.

3.3. Superalloy results

The results of push-pull tests with the superalloy show noticeable differences in comparison with stainless steel results (Fig. 6): the loading branches have an important quasi-linear portion after the inversion points; the evolution of the circumferential strain shows a wider cycle and the ratchet phenomenon is also obvious, with a slight dissymmetry due probably to a sample misalignment. This material displays essentially a phenomenon of softening, after a slight hardening effect during the first cycle [8, 11].

After the curve fitting, the results show that the variation of the modulus M_E is continuous, like for the stainless steel, with a slow variation at the beginning (Fig. 7). But

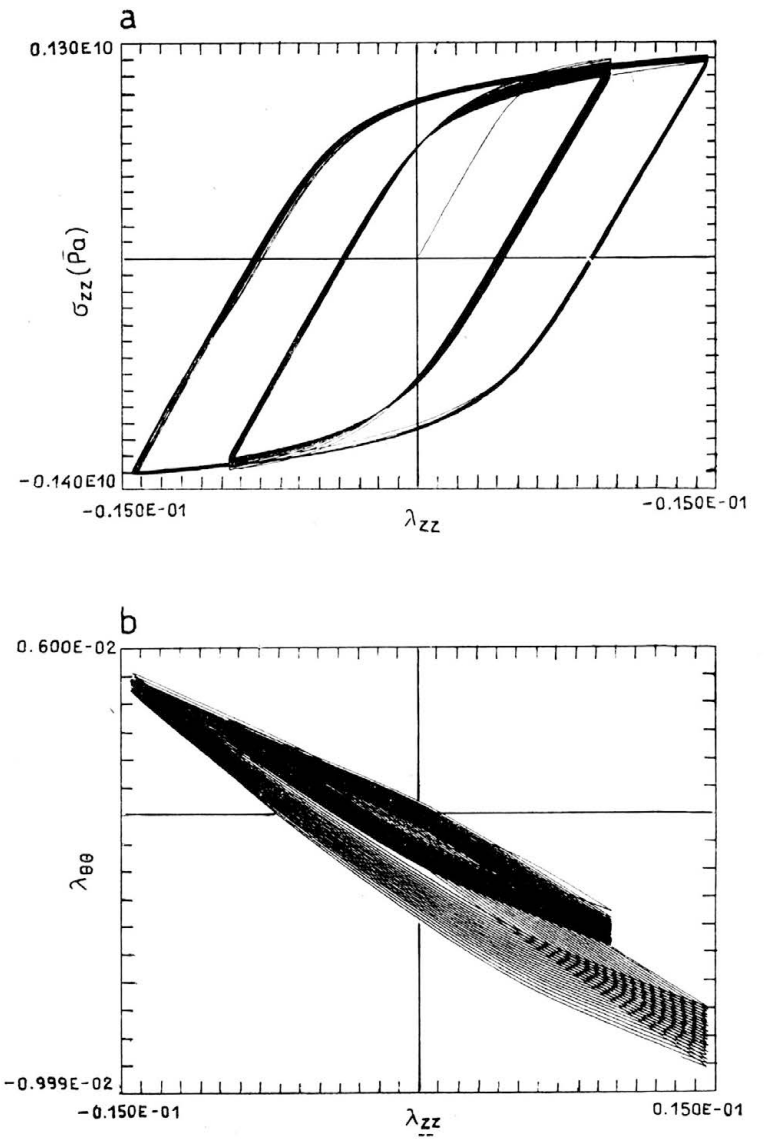

FIG. 6. Push-pull test. Axial stress a) and circumferential strain b) versus axial strain. Superalloy.

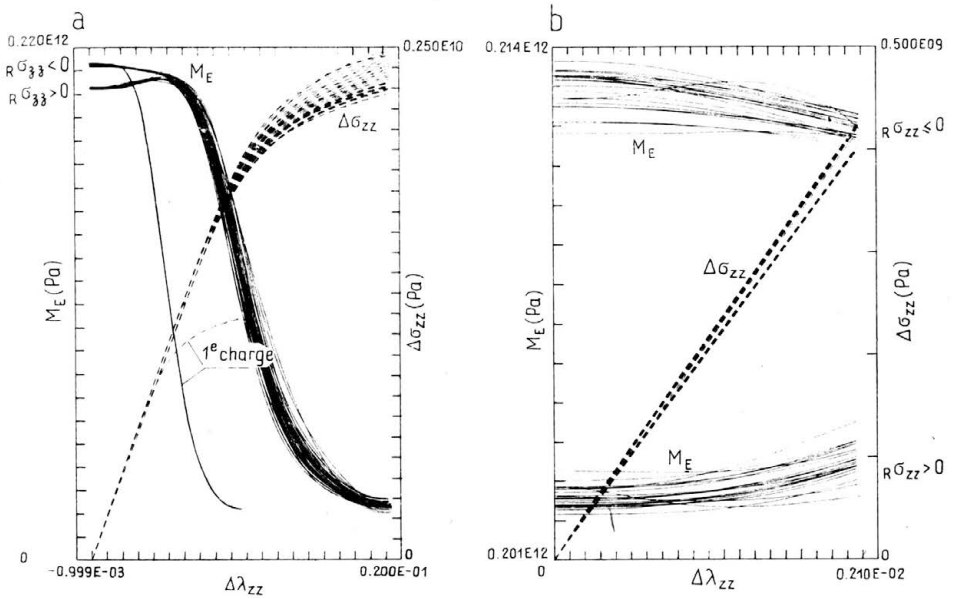

FIG. 7. Push-pull test. Variation of stress difference $\Delta\sigma_{zz}$ and modulus M_E for the small cycles, a) whole interval 0–1%; b) enlargement of interval 0–0.2%. Superalloy.

the curves separate into two distinct parts during a strain interval of 5.10^{-3}: the upper one corresponds to the loading branches whose origin is in compression and the lower one corresponds to the loading branches whose origin is in traction. The first loading branch shows a M_E initial value identical with those of the branches beginning in compression.

This result can be explained by a Young's modulus E depending on the stress invariant, say for simplicity in a first order, on the first stress invariant I. If we admit that E decreases with the increase of I and decreases more rapidly when I_σ is positive, then the M_E evolution of Fig. 7 can be explained. We will see later in the text that microstructural phenomena can justify this hypothesis. To compare the results of the two materials it has to be noticed that the strength of the superalloy is three times greater than that of the stainless steel; thus the dependency of I_σ for E can exist for the stainless steel but is negligible.

The variation of the coefficient C_v (Fig. 8) also shows a clear separation of the loading branches into two groups, not only in the quasi-elastic region but also in the quasi-plastic region: for the branches whose reference point is in transition, the coefficient C_v varies from 0.28 to 0.49, and for the branches whose reference point is in compression, the coefficient C_v varies from 0.30_5 to 0.45. A quasi-plastic state in compression shows almost no volume variation, as in the quasiplastic traction states the volume variation is obviously not null.

The results of a pure torsion test are given in Fig. 9 with the $\Delta\sigma_{\theta z}$ and the M_μ variations for only the first group of small cycles ($\pm 0.80\%$). All the branches, with the exception of the first loading branch, have the same M_μ evolution, according to isotropic materials. The evolution is of the same type as the M_E evolution of the branches beginning in a traction state. On the other hand, the M_μ evolution of the first loading branch is of the same type

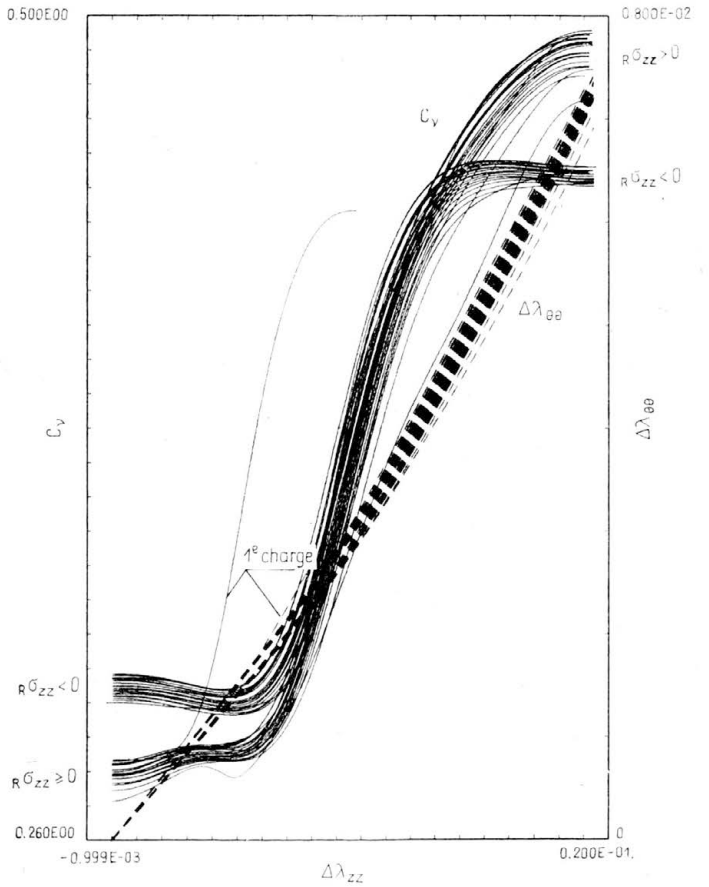

FIG. 8. Push-pull test. Variation of circumferential strain difference $\Delta\lambda_{\theta\theta}$ and coefficient C_v versus axial strain difference $\Delta\lambda_{zz}$. Superalloy.

as the M_E evolution of the branches beginning in compression. As for the modulus M_E, the variation of the M_μ modulus can be explained by a dependency of the Lamé's coefficient on the stress invariants; this will be developed later.

In summary the data characterizing the tangential elastic behaviour are given in Table 1. The error interval is determined by the dispersion of the value for all branches. For the neutral state we have only one value; we check that, at a relative accuracy of 1.3%, the three values of the neutral state are consistent since we obtain by Eq. (3.2) $\mu^* = 82.9$ GPa. A valuable modelization of the two elastic parameters will be given later, after an analysis at the microstructural scale.

3.4. Attempt of explanation at the microstructural scale

To confirm the preceding results analysis, it is of interest to try finding, at the microstructural scale, qualitative explanations of the properties revealed at the macroscopical scale.

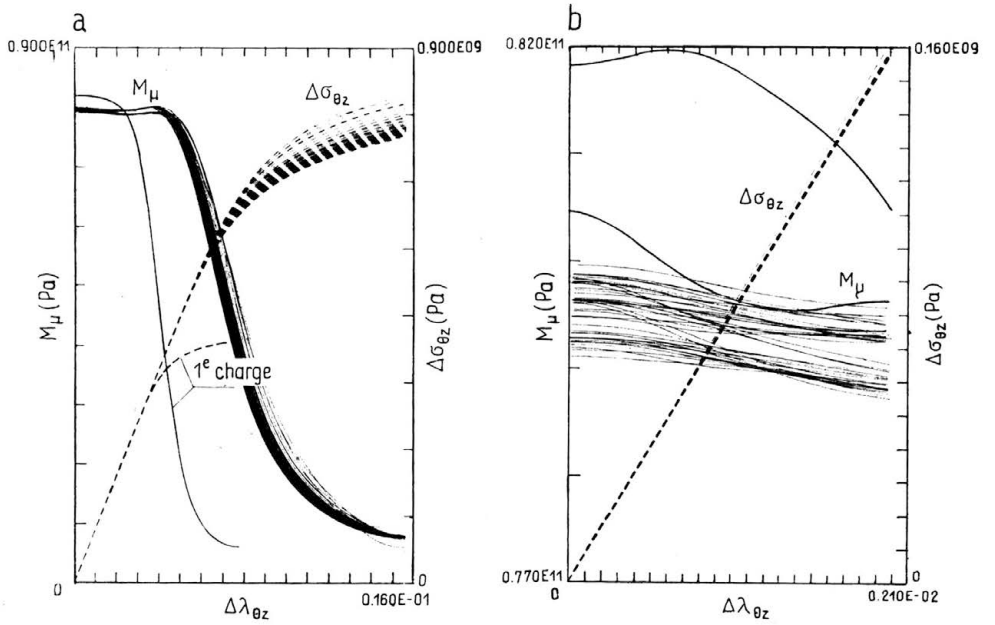

FIG. 9. Cyclic torsion test. Variation of stress difference $\Delta\sigma_{\theta z}$ and modulus M_μ versus shear strain difference, a) whole interval 0–1.6%; b) enlargement of interval 0–0.2%. Superalloy.

Table 1.

state	stress (MPa)	E (GPa) (mes.)	ν (mes.)	μ (GPa)		λ (GPa) (cal.)
				(mes.)	(cal.)	
A	0	212.7	0.283	81.8	82.9	108.1
B	+1140	202.7±0.5	0.278±0.005	/	79.3	99.3
C	−1250	212.7±0.8	0.305±0.005	/	81.5	127.5
D	± 700	/	/	79.5±0.4	/	/

a. Immediate irreversibility of the deformation. For polycrystalline materials, the crystalline lattice of each grain has any sort of orientation with regard to the external solicitation. Thus it is possible to imagine that there always exists a "sensitive grain" in which a preexisting dislocation may unpin for a very low external stress variation due to its particular position in that grain. When the external stress continues to increase, other preexisting dislocations in other grains will unpin and further, new dislocation loops will be created, by the mechanism of Franck–Read sources for example. This progressive phenomena explains the nonlinear aspect we obtain for the stress-strain curve at the macroscopical scale.

Theoretically it is possible to imagine the existence of a threshold under which no dislocations will unpin, the material deformation being due only to the crystal lattice deformation with its imperfection and to moving dislocations without unpinning. But

the value of this threshold is of a very low level, with no comparison to the value used in the classical elasto-plastic behaviour (for example [12]).

This immediate irreversibility of the deformation is well known by metallurgists. Instead, for example, fifteen years ago VELLAIKAL [13] claimed clearly in the introduction of his article: "It is well known that high sensitivity stresses measurements or dislocation etch-pit techniques can detect small plastic strains well below the macroscopic yield stress in many metals and alloys". A great number of measurements was made on copper which has the same FCC structure as the stainless steel: for mono- or polycrystals of copper as for aluminium solid dilutions in copper, a few authors have made conspicuous the fact that irreversible dislocation movements appear for bending stresses of a few g/mm^2 [13 to 16], which represents one thousandth of the ultimate strength. We notice last the work done by ARGON and BRYDGES [17]: the authors define for monocrystalline copper an elastic limit of 7 g/mm^2 and a multiplication stress, beyond which the dislocations creation multiplies, of a value of 20 g/cm^2.

All these results are now confirmed by in situ dynamical observations with an electron microscope. For example we can refer to the work done by FUJITA and co-authors [18, 19].

b. Elastic tangential behaviour. Consider first the case of stainless steel which is simpler. After any inversion state the tangential modulus of the loading branches is the same, at a relative accuracy of one per cent, whatever the amplitude of the cycles and the stress level; however, the latter increases about 40% due to the consolidation phenomenon. An analysis at the microscopical scale shows the reality of this intrinsic property of the modulus: it is nothing other than the deformation modulus of the initial polycrystal with its defaults and its network of preexisting dislocations.

In fact consider what happens around an inversion state. Before an inversion, there exists a given dynamical state of moving dislocations and, in particular, some dislocations leave one part of a joint, cross the subgrain and pile up on the opposite side of the subgrain boundary or on internal barriers. When the solicitation changes its sign, all this dynamical state has the tendency to change direction and the dislocations will move in the opposite direction [18]. Thus, during a short time, the dislocation speeds drop to zero and change sign. At that time the rigidity of the material is that of the polycrystal without dislocation unpinning.

For the superalloy the results seem more complicated: on one hand the modulus after an inversion seems to depend on the stress state and on the other hand the evolution of the modulus does not always have a parabolic variation near the origin. The dependency of the modulus with regard to the stress state is well known by the acousticians who have made conspicuous the wave speed variation with different stress conditions [20, 21]. This phenomenon can be intuitively explained by the equilibrium between attractive and repulsive forces acting on individualized atoms. Thus the evolution of the total force acting between two atoms with regard to their distance is represented by the classical atomic interaction diagram (Fig. 10) [22]: if we want to increase the distance between the two atoms, the total force must be attractive and has to increase with the distance and passes theoretically through a maximum before decreasing. On the contrary, to reduce the distance it is necessary to exert a compressive fort which increases regularly with the decrease of the

distance. The deformation modulus of this simple system is proportional to the slope of this curve; due to its shape the slope varies more rapidly in the attractive state than in the compressive state for the same force interval. This may explain the modulus variation near the origin.

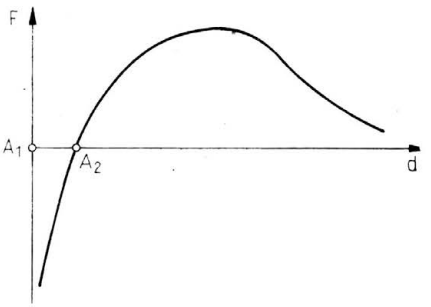

FIG. 10. Atomic interaction diagram.

After an inversion in a traction stress state, the modulus has a small value; when the stress decreases the material rigidity is a consequence of two opposite phenomena: an increase of polycrystal rigidity due to the decrease of the stress (Fig. 10) and a decrease due to the moving dislocations. These two combined phenomena give the quasisinusoidal evolution of the M_E curves (Fig. 7a). If the inversion takes place in a compressive state the influence of the stress state and of the moving dislocations will be of the same type, a decrease of the rigidity, and we obtain a parabolic evolution like those of the stainless steel. When the influence of the moving dislocations is predominant, the two groups of M_E ($\Delta\lambda_{zz}$) curves join. In the frame of this explanation the quasi-plateau of Fig. 9a has to be interpreted as a very flat sinusoidal portion; in fact this group of curves joins the first loading curve transformed by affinity. The first loading curves (Figs. 7 and 9) belong to the curve group beginning in a compression state; this in accordance with the shape of the atomic interaction diagram: the slope in the compressive state is almost equal to the value at the origin (Fig. 10).

These phenomena must also influence stainless steel behaviour; but the stress variation being about three times smaller than for the superalloy, the effects are too small to be noticeable with regard to the accuracy of our test device.

The preceding analysis allows us to modelize the stress influence on the elastic parameters, expressed by the Lamé's coefficients λ and μ for which the theory [5, 23] predicts a possible stress variation by the stress invariants (Table 1).

A variation of the λ coefficient with only the first stress invariant I_σ is sufficient to modelize the results as follows:

$$\lambda = \lambda_0 \exp\left(-\frac{I_\sigma}{p_0}\right)^{n_0}. \tag{3.4}$$

With $\lambda_0 = 108.1$ GPa, $p_0 = 2.40$ GPa and $n_0 = 3$, we obtain:

state	A	B	C
λ (GPa)	108.1	97.1	124.5

It is not useful to try finding a more complicated stress dependency, due to the small amount of experimental results.

The variation of the μ coefficient is more complex: the maximum value is obtained for $I_\sigma = II_{\bar{\sigma}} = 0$ and is near the value obtained in the compression state. We admit that μ varies with the second invariant of the stress deviator $II_{\bar{\sigma}}$ between the maximum value and a value depending on the stress phase ξ such that

$$\mu = \mu_0 - c_1 II_{\bar{\sigma}}(1+\cos 3\xi)^{n_1}. \tag{3.5}$$

With the four experimental data, a good approximation is given by:

$$\mu_0 = 81.8 \text{ GPa}, \quad c_1 = 10/3, \quad n_1 = 1/6.$$

Using Eqs. (3.4) and (3.5) in the constitutive scheme, the modelization of the superalloy push-pull test (Fig. 6) gives a M_E evolution (Fig. 11) which is very similar to the experimental results (Fig. 7).

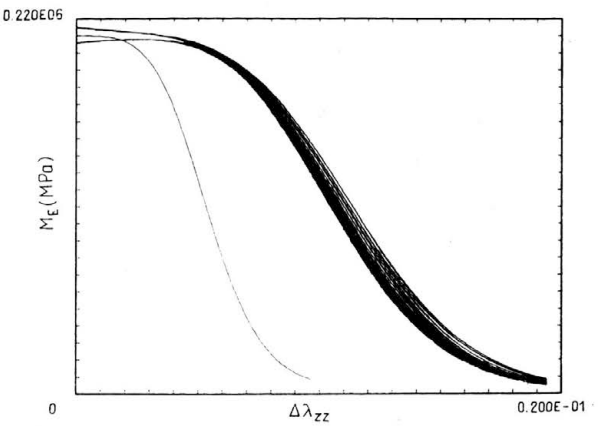

FIG. 11. Modelization of the cyclic push-pull test (see Fig. 7a). Variation of the modulus M_E. Superalloy.

4. Small cycle described in a large cycle

The discrete memory notion was made conspicuous by the analysis of the loading branches in the $\Delta\sigma$, $\Delta\lambda$ axes: at the beginning all the branches are identical and they differ afterwards due to the presence of strain hardening. A solicitation path describing a small cycle into a large cycle makes this notion of discrete memory more obvious. To avoid the influence of the strain hardening phenomenon, this test is run after the saturation state is obtained.

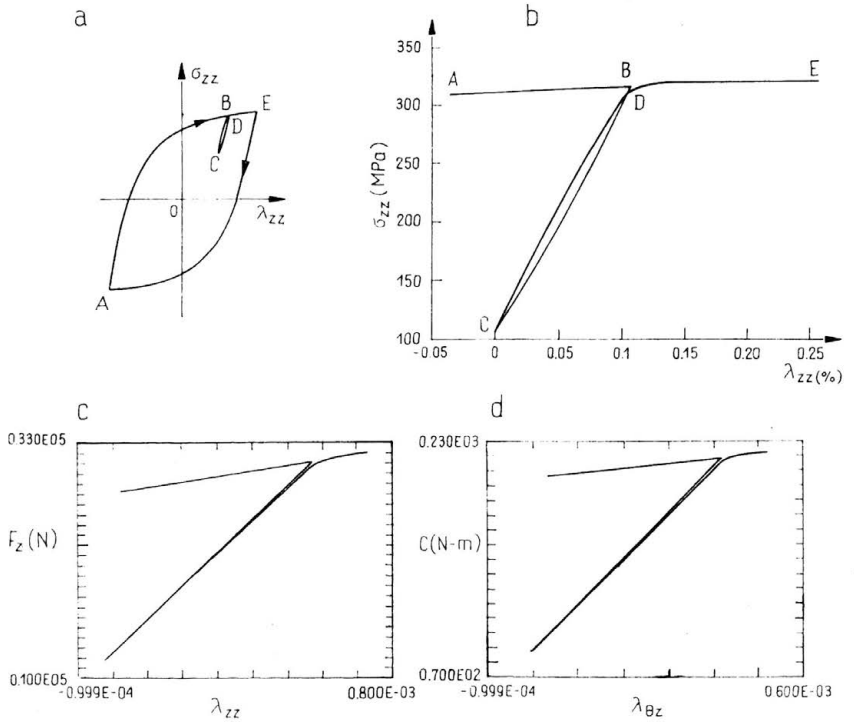

FIG. 12. Small cycle described in a large cycle, b) push-pull test; c) and d) proportional traction-torsion test.

In that case the constitutive scheme predicts a behaviour described by an equation of the following type:

$$\sigma - {}_R\sigma = f(\lambda - {}_R\lambda).$$

Consider a stabilized cycle AE, in which we inscribe a small cycle BCD (Fig. 12a). Along the branch CDE the reference state $({}_R\sigma, {}_R\lambda)$ will change abruptly at point D: for the arc CD the reference state is defined by the state of point C and for the arc DE by the state of point A; so the arc DE is the continuation of the branch AB.

The experimental curve describing such a push-pull type test is given in Fig. 12b. This is analogical with the recording chosen to avoid the truncation given by the ordinary digital recording. We see first that the solicitation describes a small cycle which is closed and has a finite area. Secondly we see that at point D the branch CDE shows a very rapid change in the curvature. At a relative accuracy of 1% of the stress we may say that the branch CDE is constituted by two arcs with a discontinuous slope change at point D and that arc DE is the continuation of the branch AB.

This result is confirmed by another small cycle described in a large cycle: Figs. 12c and 12d show such a cycle obtained this time by a digital recording with a combined solicitation of proportional traction and torsion. The same properties as with the preceding cycle are made conspicuous for the axial force variation as for the torque variation.

From the view point of the macroscopical constitutive scheme the notion of discrete

memory is introduced by the properties of the heuristic model of springs and sliders [4, 5]. If this notion has really a meaning, we have to find its correspondence at a microstructural scale. In other words, the notion of discrete memory must be stamped in some microstructural phenomena.

It seems to be possible to give a satisfactory response making use of the analysis of the dislocations mechanisms. Different authors in metallurgy (for example [24, 25]) refer, like authors in the field of mechanics, to the original work done by MASING [1]. They make a direct parallel between the rheological model with springs and sliders and the individual mechanisms of dislocation creation or movement, classified by a threshold of activation (in energy for example). The individual mechanisms have to be understood in a broade sense, that is mechanisms of different types as the same mechanisms at different positions and/or orientations with regard to obstacles (grain or subgrain boundary, default or imperfection). Thus MUGHRABI [2] introduces a composite model of the material with walls of high dislocations density and channels of low dislocations density, each region characterized by a threshold for the activation of the dislocations: this model (Fig. 4 of [24]) is identical to the two layers model analysed by us (Fig. 4b [5] or Fig. I.12 [8]). Otherwise HOLSTE and BURMEISTER [3] introduce a model at a scale of dislocations structure, called half-macroscopic volume, whose properties are continuously distributed.

Thus the foundation of the discrete memory notion would befound in the dislocation mechanisms activated or not. Coming back to the small cycle described in a large cycle, it is possible to give an explanation from the microstructural point of view. Until point B (Fig. 12.b) a great number of mechanisms of dislocation creation or dislocation movement become progressively activated, the most energetic one having a threshold T_{max}. After inversion, all these mechanisms will stop and have the tendency to activate in the reverse direction beginning with those of lower energy. Until point C only mechanisms of threshold lower than T_{min} are activated. After the inversion C these mechanisms stop again and have the tendency to change direction, that is the same direction as during the initial solicitation AB. As we approach gradually point D, which is identified with point B, the memory of the dislocation history occuring during the path BC is erased. At point D all the memory of the events comprised between the threshold 0 and T_{min} corresponding to the path BCD is erased and the material is exactly at the same situation as before the inversion B. If we continue the solicitation to DE, the material will activate mechanisms of dislocation of thresholds greater than T_{max}, as if we had extended path AB directly to path BE, without doing the small cycle BCD.

In summary, at the microstructural scale the activated dislocation mechanisms will jump, along the path CDE at point D, from those in the threshold interval $0 - T_{min}$ to those in the threshold interval $0 - T_{max}$. This jump corresponds on the macrostructural scale to the jump of the reference state $({}_R\sigma, {}_R\lambda)$ and the jump of the reversible power.

The preceding explanation has to be taken, in the author's opinion, as a predictive explanation since there does not exist at the present time any direct experimental observation of this phenomenon. But due to the powerful possibilities of the microscopical technique it may be possible now to verify the author's statement by direct in situ microscopical observations.

5. Shape of the loading surface

The loading surface defines an asymptotic limit stress state in the sense that the representative point of the material stress state never reaches it [11]. A material subjected to a strain hardening (or softening) phenomenon is characterized by a loading surface moving as this phenomenon takes place. We make the hypothesis, as a first approximation, that its shape does not change; therefore in the following we will deal only with the loading surface of the pure hysteresis behaviour σ_a. We recall that the constitutive scheme expresses the constitutive equation as a sum of partial stress [4]; thus for a material subjected to strain hardening:

$$\sigma = \sigma_a + \sigma_g, \tag{5.1}$$

where σ_a corresponds to pure hysteresis and σ_g to strain hardening; for the virgin material σ_g is null and $\sigma = \sigma_a$.

Due to the experimental data available, we consider only cylindrical surfaces which are characterized by the section in the deviatoric plane $\hat{II}_{\bar{\sigma}_a}(\xi)$, where $\hat{II}_{\bar{\sigma}_a}$ is the limit value of the second invariant of the stress deviator $\bar{\sigma}_a$ and ξ is the phase angle. The stress limit values for pure hysteresis behaviour in traction, compression and torsion are respectively Y_0, Z_0 and S_0, and we have

$$Y_0 = \sqrt{3}\,\hat{II}_{\bar{\sigma}_a}(0), \quad Z_0 = \sqrt{3}\,\hat{II}_{\bar{\sigma}_a}\left(\frac{\pi}{3}\right), \quad S_0 = \hat{II}_{\bar{\sigma}_a}\left(\frac{\pi}{6}\right).$$

These values cannot be determined directly by experimental measurements due to the presence of strain hardening (or softening); with symmetrical cyclic tests it is possible to use a method of extrapolation of the values at the inversion points and the limit values are defined by

$$\hat{II}_{\bar{\sigma}_a} = \lim_{N \to 0} \hat{II}_{\bar{\sigma}}(N), \tag{5.2}$$

where N is the number of half-cycles [8, 11].

For the stainless steel the experimental data obtained with the strain-controlled symmetric cyclic tests give the following mean value for traction and compression:

$$Y_0 = Z_0 = 300 \pm 9 \text{ (MPa)}.$$

We have to notice a slight systematic difference between traction and compression, but within the dispersion interval of all the experimental values. The torsion tests give

$$\sqrt{3}\,S_0 = 281 \pm 10 \text{ (MPa)}.$$

The dispersion intervals of these two values are tangent; due to this small difference it is possible to admit a global mean value and thus a von Mises loading surface; the mean value retained is

$$\langle Y_0 \rangle = \langle Z_0 \rangle = \sqrt{3}\,\langle S_0 \rangle = 294 \pm 10 \text{ (MPa)}$$

the value and its uncertainty interval (at 95%) are statistically defined with all the available test results.

For the superalloy only one test is available for each of the three values and we obtain

$$Y_0 = 1150, \quad Z_0 = 1250, \quad \sqrt{3}\,S_0 = 1170 \text{ (MPa)}.$$

As the maximum relative difference is equal to 9%, we have to admit that a von Mises loading surface cannot correctly represent these results. We choose a cylindrical surface whose section in the deviatoric plane is given by

$$\hat{II}_{\sigma_a}(\xi) = \hat{II}_{\bar{\sigma}_a}(0)[1 + c_2(1 - \cos 3\xi)^{n_2}]. \tag{5.3}$$

This section is similar to the one proposed by STUTZ [23] for granular materials. The three coefficients $\hat{II}_{\bar{\sigma}_a}(0)$, c_2 and n_2 are directly determined by the three experimental values and we have

$$\hat{II}_{\bar{\sigma}_a}(0) = 659 \text{ (MPa)}, \quad c_2 = 0.0256, \quad n_2 = 1.33.$$

This dissymmetry, experimentally established, obliges us to verify the possibility of modifying the unidimensional symbolic model of springs and sliders in such a way as to include the case of dissymmetry in traction and compression.

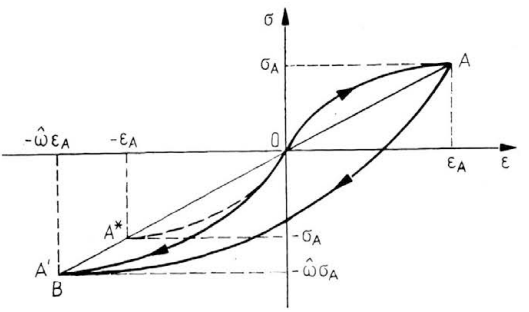

FIG. 13. Loading and unloading branches of the dissymmetric symbolic model — the notion of dissymmetry factor $\hat{\omega}$.

The proposed dissymmetric model differs from the symmetric one only by the fact that each slider is characterized by two thresholds e^+ and e^- depending on the direction of sliding, the dissymmetry factor $\hat{\omega} = e^-/e^+$ being kept the same for all sliders; on the other hand, to guarantee the continuity around the origin, the spring modulus must be kept the same for each direction. An analysis identical to the one done for the symmetric model shows that this proposed model has the same fundamental properties as the original one [4, 8]:

a) All the loading arcs $\sigma(\varepsilon)$ are similar to each other (Fig. 13); they are defined by a general equation:

$$\sigma - {}_R\sigma = \omega f\left(\frac{\varepsilon - {}_R\varepsilon}{\omega}\right). \tag{5.4}$$

Three different cases are recognized, with a given value of the Masing similarity coefficient ω:

$\omega = 1$ first loading in the traction direction,
$\omega = \hat{\omega}$ first loading in the compression direction,
$\omega = 1 + \hat{\omega}$ second loading in any direction,

we verify that this includes the symmetrical case for the dissymmetry factor $\hat{\omega}$ equal to unity.

b) We verify simply that the "help function" W_L takes the same value at points A, A' and B (Fig. 13); thus the use of the algorithm to define functionals does not change.

c) The state of the symbolic model is represented by the same topological diagram, the only difference being the fact that the representative points of each couple move on straight lines having a slope not parallel to the spring deformation axis; this slope depends only on the dissymmetry factor $\hat{\omega}$.

d) The thermodynamical variables rates have also a dissymmetrical evolution. This is made conspicuous by the diagrams of Fig. 14 corresponding to a strain-controlled symmetrical solicitation with $\dot{\varepsilon} = \pm 1$. For the second loading type branches, the evolution

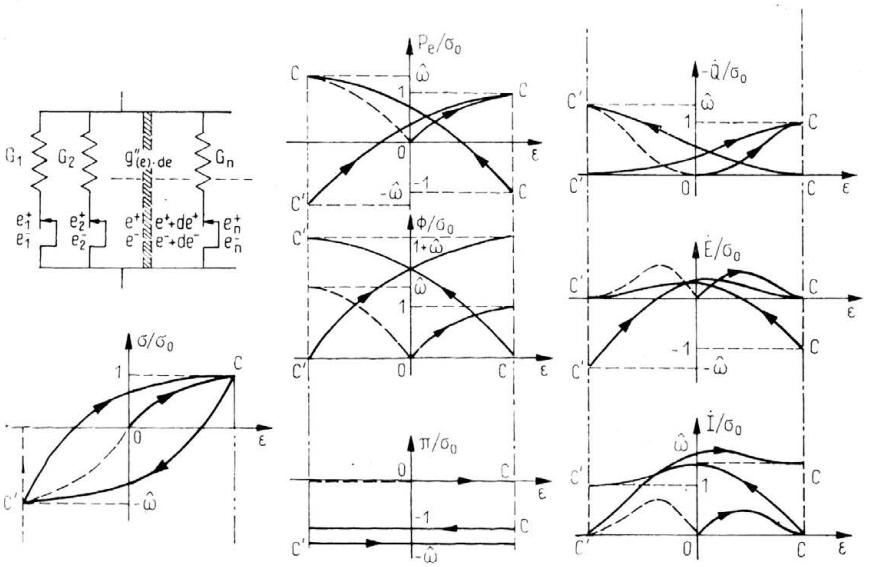

FIG. 14. The dissymmetric symbolic model. Evolution of the thermodynamical variable rates for $\dot{\varepsilon} = \pm 1$ (P_e power of external forces, E internal energy, I disorder variable, ϕ intrinsic dissipation, π reversible power, $-\dot{Q}$ heat rate associated with the irreversible phenomena [4, 5].

of some rates depends on the solicitation sign; this is a consequence of the fact that the stable value in the quasi-plastic state of the heat rate $-\dot{Q}$ is different in traction and in compression. Thus another parameter Ω, taking the values 1 or $\hat{\omega}$, has to be introduced to give the expression of the thermodynamical rates [8].

e) The extension from the unidimensional symbolic model to the three-dimensional case is not simple. For convenience it is possible to introduce a relation between the dissymmetry factor $\hat{\omega}$ and the shape of the loading surface |8|. This procedure consists in defining the dissymmetry factor as a function of the stress phase ξ through a stress ratio:

$$\hat{\omega}(\xi) = \frac{\hat{II}_\sigma(\xi)}{\hat{II}_\sigma(0)}. \tag{5.5}$$

Thus a similarity coefficient can be again defined in the algorithm by a simple "if" condition:

for an arc of the first loading type $\omega = \hat{\omega}(\xi)$,

for an arc of the second loading type $\omega = \hat{\omega}(\xi)+\hat{\omega}(\xi+\pi)$.

As we see, this includes the simplest symmetrical case of the von Mises loading surface with the similarity coefficient equal to 1 or 2. This procedure has to be taken only as a preliminary proposition. A complete study of this problem exceeds largely the frame of this article; it is related to a recent work presented by GUELIN *et al.* [24 to 26].

Finally we have to emphasize that, by taking into account a nonaxisymmetrical loading surface in the preceding works as in this one, the coupling between the mechanical and the thermodynamical aspects of the constitutive scheme is made clearly conspicuous.

6. Concluding remarks

The pure hysteresis phenomenon is recognized as the leading phenomenon in solid behavior. It introduces the notion of discrete memory in the constitutive scheme. The validity of the discrete memory notion is confirmed by the fact that this notion has a microstructural support at the dislocations scale.

It has been shown that the stress-strain curves present no discontinuities, at least to the third order. The notion of boundary between an elastic and a plastic domain does not correspond to reality, at least for the superalloy and the stainless steel tested. Thus the material deformation, in the range of engineering stresses, has to be considered as irreversible from the beginning; metallurgists state that such a boundary may exist but at a very low stress value of magnitude 1/10 MPa. Moreover, the properties of the material are restored after each inversion state, as it is made conspicuous by the results at the macroscopical scale; a microstructural explanation at the dislocation scale is also given. Consequently, the notion of elastic behaviour as an approximation of the real material behaviour has to be considered as a tangential behaviour at the origin of each loading branch, just after an inversion state.

The introduction of an axisymmetrical loading surface made more obvious the coupling in the constitutive scheme between the mechanical and the thermodynamical aspects. A complete solution of this problem is not simple and is still a partially open problem, for example with regard to the question of uniqueness.

The results obtained show that there are no contradictions between the prediction of the discrete memory constitutive scheme and the results at the macroscopical scale. Moreover, some explanations of the constitutive scheme main properties can be found at a microscopical scale. Further studies have to be done to consider a larger experimental field. On one hand, other types of materials have to be tested, and aluminium alloys seem to be particularly interesting. On the other hand, a systematic parallel between macroscopical and in situ microscopical tests appears to be possible now. The comparisons which are possible to obtain present a special interest to confirm, or infirm, the hypotheses and thus to improve and develop the discrete memory constitutive scheme.

Acknowledgement

This work was financially supported in part by the "Direction des Etudes et Recherches" of "Electricité de France", the "Centre National de la Recherche Scientifique" (under contract GRECO "Grandes Deformations et Endommagement") and the "Ministere de la Recherche et de la Technologie" (under contract G.I.S. "Rupture à chaud").

References

1. G. MASING, *On Heyn's hardening theory of metals due to inner elastic stresses*, Wiss. Veroff. Siemens Konzern, 3, 231–239, 1923.
2. H. MUGHRABI, *Dislocation wall and cell structures and two long-range internal stresses in deformed metal crystals*, Acta Metall., **31**, 9, 1367–1379, 1983.
3. C. HOLSTE, H. J. BURMEISTER, *Change of long range stresses in cyclic deformation*, Phys. Stat. Sol. (a), **57**, 269–280, 1980.
4. P. GUELIN, *Remarque sur l'hystérésis mécanique 1. Les bases d'un schéma thermomécanique à structure héréditaire*, J. Mécanique, **19**, 2, 217–247, 1980.
5. B. WACK, J. M. TERRIEZ, P. GUELIN, *A hereditary type, discrete memory, constitutive equation with applications to simple geometries*, Acta Mech., **50**, 9–37, 1983.
6. J. M. BOISSERIE, P. GUELIN, J. M. TERRIEZ, B. WACK, *Applications of a hereditary constitutive law of discrete memory type*, J.E.M.T., **105**, 155–161, 1983.
7. D. KUJAWSKI, V. KALLIANPUR, E. KREMPL, *An experimental study of uniaxial creep, cyclic creep and relaxation of AISI type 304 stainless steel at room temperature*. J. Mech. Phys. Solids, **28**, 129–148, 1980.
8. S. HAN, *Le comportement d'hystérésis des solides et sa description par un schéma à mémoire discréte: le cas des aciers inoxydables*, Doctor's Thesis, University of Grenoble, 1985.
9. M. N. ELLEUCH, S. HAN, B. WACK, *Experimental verification of a discrete memory constitutive model for 316 stainless steel*, 7th SMIRT, L 10/3, 369–376, 1983.
10. B. WACK, *Second and third-order effects in the torsion of circular tubes and rods*, J. Mécanique, **20**, 4, 737–787, 1981.
11. S. HAN and B. WACK, *Discrete memory description of strain hardening and softening with application to stainless steel and superalloy*, Res Mechanica (to appear 1985).
12. J. L. CHABOCHE, G. ROUSSELIER, *On the plastic and viscoplastic constitutive equations*, P. I et II ASME, **59**, ed. G. Baylac, 33–55, 1982.
13. G. VELLAIKAL, *Some observation on microyielding in copper polycrystals*, Acta Metallurgica, **17**, 1145–1154, 1969.
14. F. W. YOUNG, *Elastic-plastic transition in copper crystal as determined by an etch-pit technique*, J. Appl. Physics, **32**, 10, 1815–1820, 1961.
15. F. W. YOUNG, *On the yield stress of copper crystals*, J. Appl. Physics, **33**, 3, 963–969, 1962.
16. R. F. TINDER, J. WASHBURN, *The initiation of plastic flow in copper*, Acta Metallurgica, **12**, 129–137, 1964.
17. A. S. ARGON, W. T. BRYDGES, *Deformation of copper in easy glide*, The Philosophical Magazine, **18**, 154, 817–837, 1968.
18. H. FUJITA, *In situ deformation by high voltage electron microsopy*, 9th Intl. Cong. on Electron Microscopy, III, 355–366, 1978.
19. H. FUJITA, *Behaviors of individual dislocation in* Cu-9 *at* % Al *alloys under reverse stress*, J. Physical Society of Japan, **38**, 5, 1342–1348, 1975.
20. D. LAZARUS, *The variation of the adiabatic elastic constants of* KCl, NaCl, CuZn, Cu *and* Al *with pressure to* 10 000 *Bars*, Physical Review, **76**, 4, 545–553, 1949.
21. S. TAKAHASHI, *Change of the ultrasonic characteristic with stress in some steels and aluminium alloys*, J. Materials Science, **13**, 843–850, 1978.

22. C. KITTEL, *Introduction to solid state physics*, John Wiley and Sons Inc., 86–98, 1976.
23. P. STUTZ, *Contribution à l'étude de la loi rhéologique des milieux pulvérulents*, Thèse d'Etat, Grenoble 1971.
24. P. GUELIN, W. K. NOWACKI, P. PEGON, *Etude des schémas thermomécaniques à mémoire discrete: bases physiques et formalisme*, V-ème Symposium Franco-Polonais, Rydzyna, 1984; (to appear Arch. Mech.).
25. P. PEGON, P. GUELIN, *On thermomechanical Zaremba schemes of hysteresis*, Res Mechanica (to appear 1985).
26. D. FAVIER, P. GUELIN, P. PEGON, *Schémas thermomécaniques de l'hystérésis et résultats récents en grandes déformations élastoplastiques*, Cahiers du Groupe Français de Rhéologie, N° spécial (à paraître).

INSTITUT DE MECANIQUE DE GRENOBLE
DOMAINE UNIVERSITAIRE, SAINT MARTIN D'HERES, FRANCE.

Received December 27, 1985.